Molecular electronics: controlled manipulation, noise and graphene architecture

Tewari, S.

2. Human-machine augmented system to control single atoms

A new way to control individual molecules and mono-atomic chains is devised by preparing a human-machine augmented system in which the operator and machine are connected by a real-time simulation. Here a 3D motion control system is integrated with an ultra-high vacuum (UHV) low temperature scanning tunneling microscope (STM). Moreover we coupled a real-time molecular dynamics (MD) simulation to the STM which provides a continuous visual feedback to the operator during atomic manipulation. This allows the operator to become a part of the experiment and to make any adaptable tip trajectory which could be useful for atomic manipulation in 3 dimensions. The strength of this system is demonstrated by preparing and lifting a mono-atomic chain of gold atoms from the Au(111) surface in a well-controlled manner. We also show here a new geometric procedure to infer the ad-atom positions and therefore information about the substrate atoms which are not easily visible in clean metallic surfaces like gold. This method enables a new controlled atom manipulation technique which we will refer to as point contact pushing (PCP) technique. Finally we discuss the effect of unknown spring stiffness of STM tips in addition to the unknown atomic configuration of tip apex on the accuracy of atomic manipulations.

The work is done in collaboration with - Jacob Bakermans[1], Christian Wagner[2], Federica Galli[1] and Jan M. van Ruitenbeek[1]
[1]Huygens-Kamerlingh Onnes Laboratorium, Universiteit Leiden, The Netherlands.
[2]Peter Grünberg Institut (PGI-3) Jülich, Germany.

2.1 Introduction

Manipulating single atoms and molecules on metal surface using STM is not new. In early 1990s, while studying the adsorption of Xenon atoms[1] on a Pt surface using STM, researchers at IBM observed that the STM tip is not only imaging the surface but also occasionally dragging the adsorbed atoms on the surface. Consequently, they found out that by bringing the tip closer to the adsorbed atoms, the van-der Waals (vdW) force between the tip and the ad-atom becomes large enough to overcome the corrugation barrier of the surface making it easier to drag the atom[1–4]. Such manipulation of atoms or molecules along the surface is called lateral manipulation (LM), and is further classified[5–7] into three types: pulling, pushing and sliding. LM is performed while using the STM in a constant current mode with a tunnel gap. LM has also been demonstrated on a single Br atom at room temperature[8] over Cu(001) surface in UHV condition. Various complex 2D nano-structures[3,9–14] have been made by manipulating single atoms and molecules and it has also been demonstrated that these LM techniques can be performed in an automated way[14,15] to create a desired 2D lattice. An independent vertical manipulation (VM) technique has also been developed which could be used in making 3D nano-structures. These vertical manipulation techniques are known to rely either on a local field emission process[16] or on multiple excitation of the substrate ad-atom vibration mode due to inelastic electron tunneling[17]. These are not considered as accurate and reliable as LM in positioning the ad-atom[15].

STM opens up the possibility of this atomic scale control because of its capability to image single atoms and molecules when they are on the surface. However, during atomic and molecular manipulation operations it is not possible to image the underlying dynamics using STM because the very tip used for imaging is also used for manipulation. The system that we have developed addresses this problem. We have

[1] Xe makes a relatively weak bond with Platinum

[1] Donald M. Eigler and Erhard K. Schweizer. In: *Nature* 344 (1990), p. 524.
[2] Joseph A. Stroscio and D. M. Eigler. In: *Science* 254 (1991), p. 1319.
[3] P. Zeppenfeld et al. In: *Ultramicroscopy* 42 (1992), p. 128.
[4] D. M. Eigler. In: *Atomic and Nanometer-Scale Modification of Materials: Fundamentals and Applications*. Ed. by Phaedon Avouris. Dordrecht: Springer Netherlands, 1993, p. 1.
[5] L. Bartels et al. In: *Phys. Rev. Lett.* 79 (1997), p. 697.
[6] Saw-Wai Hla. In: *Journal of Vacuum Science & Technology B: Microelectronics and Nanometer Structures Processing, Measurement, and Phenomena* 23 (2005), p. 1351.
[7] Gerhard Meyer et al. In: *Single Molecules* 1 (2000), p. 79.
[8] T. W. Fishlock et al. In: *Nature* 404 (2000), p. 743.
[9] Michael F. Crommie et al. In: *Science* 262 (1993), p. 218.
[10] H. C. Manoharan et al. In: *Nature* 403 (2000), p. 512.
[11] Saw-Wai Hla et al. In: *Nano Letters* 4 (2004), p. 1997.
[12] N. Nilius et al. In: *Science* 297 (2002), p. 1853.
[13] Kenjiro K. Gomes et al. In: *Nature* 483 (2012), p. 306.
[14] Marlou Slot et al. In: *Nature* 13 (2017), p. 672.
[15] Robert J. Celotta et al. In: *Review of Scientific Instruments* 85 (2014), p. 121301.
[16] In-Whan Lyo and Phaedon Avouris. In: *Science* 253 (1991), p. 173.
[17] D. M. Eigler et al. In: *Nature* 352 (1991), p. 600.

added a 3D motion control system to our STM which helps in making any required tip trajectory and combined it with a molecular dynamics (MD) simulator which simulates in real-time the manipulation process going on in the STM. The operator now receives visual feedback from this 3D molecular dynamic simulation permitting better control of the manipulation process. This is especially important in the case of 3D manipulation of single molecules and atomic chains, as there are a no pre-defined trajectories[18,19] that one can set to do those manipulations. Therefore an adaptable trajectory is the only solution where the operator can continuously communicate with the experiment through the real-time MD simulation and define the trajectory at will. This human-machine augmented system thus provides a far better control on the manipulation process and can moreover be used for 3D manipulation. In this chapter first we will start with describing the experimental setup and sample preparation technique. Later in section 2.3 we will discuss the main outline and assumptions made in preparing the real-time MD simulation. After that we report on using this system for a new lateral manipulation methodology which we refer to as point contact pushing (PCP) technique, followed by a 3D trajectory which enabled us to lift in a controlled way a chain of gold atoms above the metal surface. These atomic chains are known to show parity oscillations in conductance[20] while going from even to odd number of atoms in the chain. We detect this phenomena while controllably lifting the chain of atoms and putting it back on the surface. At the end, we will also discuss an un-addressed issue of STM tip spring stiffness and its effect on sub-atomic precision in manipulation.

2.2 Experimental setup

The experimental setup used here is a home built cryogenic STM head[21] which is cooled by an Oxford Heliox UHV system custom built for Leiden[22] The system operates at 10^{-10} mbar pressure and most of these experiments were performed at 3 K temperature (the base temperature of 300 mK was not required). A home built 3D motion control system running under LabVIEW is used to control the STM tip during manipulation. Figure 2.1 shows the schematic diagram of the complete setup with 3D motion controller and the MD real time simulator. The 3D motion control system is a simple LED tracker made with two cameras tracking the x-y and y-z motion of the LED respectively. The LED is connected on top of the operator hand (with a glove in this case), so the trajectory is drawn by the operator hand and tracked by the two cameras. Then a LabVIEW program filters and converts these x,y,z signals with proper scaling factors before sending it out to the STM tip and the simulation. The scaling factor converts approximately 10 cm of hand movement to 2 Å displacement of the STM tip. The usual imaging in STM is done using a commercial RHK SPM100 ver.8E controller. A mono-crystalline gold sample, cut in the (111) surface direction, is prepared by repeated argon sputtering and annealing cycles to obtain an atomically flat Au(111) facet showing herringbone surface reconstruction. We further prepare

[18] Matthew F. B. Green et al. In: *Beilstein journal of nanotechnology* 5 (2014), p. 1926.
[19] Philipp Leinen et al. In: *Beilstein journal of nanotechnology* 6 (2015), p. 2148.
[20] R. H. M. Smit et al. In: *Phys. Rev. Lett.* 91 (2003), p. 076805.
[21] A. F. Otte. PhD thesis. Leiden Institute of Physics (LION), Leiden University, 2008.
[22] Simon J. Kelly. PhD thesis. Leiden Institute of Physics (LION), Leiden University, 2012.

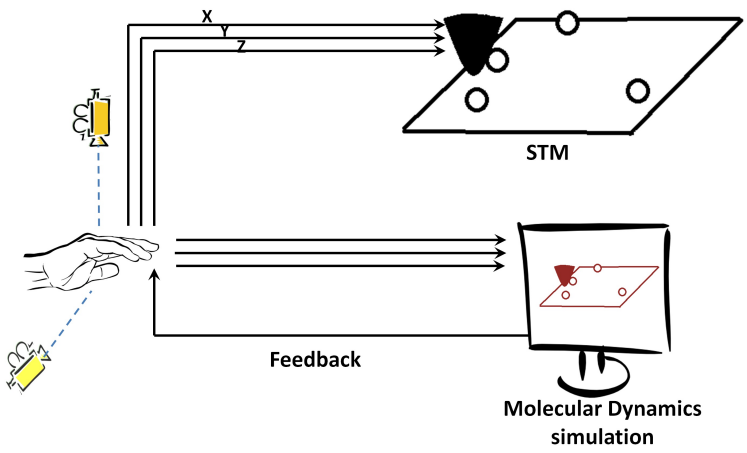

Figure 2.1: Schematic of the experimental setup. The components of the setup include a cryogenic UHV STM, a 3D motion controller and a MD simulator where the motion tracker controls both the STM and the MD simulation.

the surface at low temperature by creating a localized stress pattern[23–26] on the surface using gentle indentation of the STM tip at a spot on the surface remote from the area of investigation. This makes new crystalline (111) facets and provides straight step edges in the three crystallographic directions of Au(111) as shown in Figure 2.2(a). Additional gold atoms (ad-atoms) are deposited[27–29] on the Au(111) surface at the target sites of investigation (Figure 2.2(b)) by establishing point contact with the surface using STM tip at 100 mV bias.

2.3 Real-time molecular dynamic simulation

A conventional atomic manipulation operation using STM involves a pre-determined trajectory (controlled by the operator or by an automated procedure) of the STM tip. For example reducing the tip-sample distance and moving the tip in a desired direction assuming an isotropic nature of adsorption bonds[30] in metallic systems. In such a procedure the operator does not have any feedback while the manipulation is executed and so cannot influence the trajectory based on the complexity in the dynamics of the tip-adatom-surface system during the manipulation. In contrast, in our setup the operator receives a continuous visual feedback from real time MD simulation and can respond to different dynamics involved during the manipulation operation and

[23] D. J. Oliver et al. In: *Nanotechnology* 25 (2014), p. 025701.
[24] Francesca Moresco et al. In: *Phys. Rev. Lett.* 91 (2003), p. 036601.
[25] Francesca Moresco. In: *Physics reports* 399 (2004), p. 175.
[26] Francesca Moresco et al. In: *Applied Physics A* 80 (2005), p. 913.
[27] Saw Wai Hla. In: *Reports on Progress in Physics* 77 (2014), p. 056502.
[28] Jianshu Yang et al. In: *The European Physical Journal Applied Physics* 73 (2016), p. 10702.
[29] Sumit Tewari et al. In: *Beilstein Journal of Nanotechnology* 8 (2017), p. 2389.
[30] Phaedon Avouris. Vol. 239. Springer Science & Business Media, 2012.

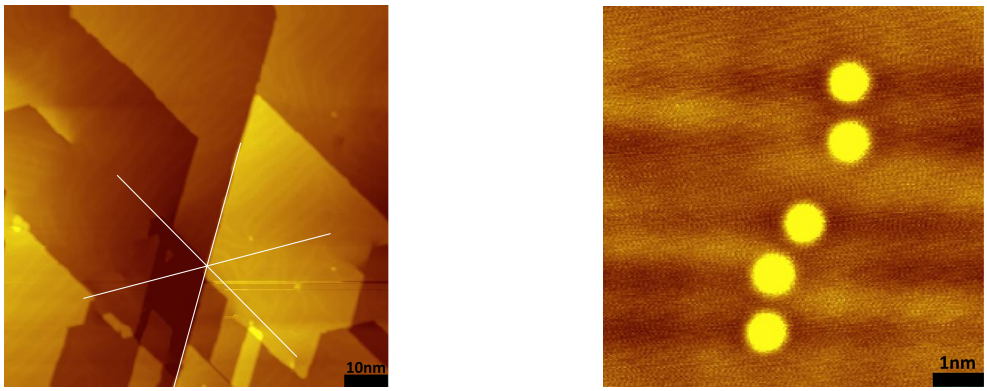

(a) (b)

Figure 2.2: (a) Atomically flat Au(111) surface with herringbone reconstruction and straight step edges in crystallographic directions prepared by stress induced lattice deformations at low temperatures, (b) Gold ad-atoms deposited on a Au(111) surface from the STM tip. Images obtained at about 3 K after the temperature was stabilized within a few mK.

alter the trajectory at will. Figure 2.1 shows how the communication between the operator and STM is made using the MD simulator. The 3D motion control sensor gives the same x,y,z signals to both the STM and the simulator simultaneously and therefore the MD simulation is required to have a minimal time delay in its response for smooth real-time operation. We do a classical MD calculation here where we ignore the electronic effects[2](which in fact give rise to the inter-atomic forces) and take the forces as coming from parametrized equations which only depend on the inter-atomic distances. The simulation we discuss in this chapter is only made for metallic systems, so in this case all the atoms involved are Au atoms. The simulation including a molecular entity along with the metallic tip and sample will be discussed in the next chapter. Here a semi-empirical potential described by Tomanek et al.[31] and Cortes-Huerto et al.[32] is used to model the Au-Au interaction. This allows for fast computation and large number of atoms involved because of its simple analytical potential functions. The potential energy is taken to be given by

$$E = -\zeta \sum_{i}^{N} \sqrt{\sum_{j \neq i}^{N} e^{-2q(r_{ij}/r_0 - 1)}} + A \sum_{i}^{N} \sum_{j \neq i}^{N} e^{-p(r_{ij}/r_0 - 1)} \tag{2.1}$$

where r_{ij} is the distance between two atoms i and j, r_0 is the equilibrium distance, and ζ, q, A and p are parameters that can be determined by fitting bulk material properties

[2] A more accurate method would be obtained by using ab-initio calculations which takes into account of both the nuclear and electronic degrees of freedom. These ab-initio calculations are however computationally very expensive and thus are not suitable for our purpose

[31] D. Tománek et al. In: *Phys. Rev. B* 32 (1985), p. 5051.
[32] R. Cortes-Huerto et al. In: *Physical Review B* 88 (2013), p. 235438.

to experimental values. The energy of Equation 2.1 consists of an attractive term (i.e., the energy decreases when the distance between two atoms decreases; the first term of Equation 2.1) and a repulsive term (the energy increases when the distance between two atoms decreases; the second term of Equation 2.1)[31]. The increase in kinetic energy for the conduction electrons trapped within two approaching atoms gives rise to this repulsive term[33], while the attractive interaction originates from the band structure and is found by a second moment approximation to the tight binding Hamiltonian[31]. From this potential energy, forces can be calculated using

$$\vec{F} = -\vec{\nabla} E. \tag{2.2}$$

The force on an atom a is therefore given by (derivation of this is given in the Appendix A.1)

$$\begin{aligned}\vec{F}_a(\vec{r}_1, ..., \vec{r}_N) = &-\zeta \frac{q}{r_0} \sum_{i \neq a}^{N} \frac{e^{-2q(r_{ia}/r_0 - 1)}}{\sqrt{\sum_{j \neq i}^{N} e^{-2q(r_{ij}/r_0 - 1)}}} \frac{(\vec{r}_a - \vec{r}_i)}{r_{ia}} \\ &- \frac{\zeta (q/r_0)}{\sqrt{\sum_{j \neq a}^{N} e^{-2q(r_{aj}/r_0 - 1)}}} \sum_{j \neq a}^{N} e^{-2q(r_{aj}/r_0 - 1)} \frac{(\vec{r}_a - \vec{r}_j)}{r_{aj}} \\ &+ 2A \frac{p}{r_0} \sum_{j \neq a}^{N} e^{-p(r_{aj}/r_0 - 1)} \frac{(\vec{r}_a - \vec{r}_j)}{r_{aj}}\end{aligned} \tag{2.3}$$

2.3.1 Implementation

The molecular dynamics simulation is written in C++ to guarantee high computational performance. Figure 2.3 shows a schematic flowchart of the simulation execution. Since providing visual feedback is one of the main objectives of the simulation, a graphics library is necessary to show visual output on the screen. For performance reasons and the ease of implementation the *Simple and Fast Multimedia Library* (SFML) is used for this purpose. We choose an object-oriented approach to keep the code well structured. A separate class is used to keep track of the individual atoms; another one to calculate energy and forces, and to integrate the equations of motion; and a third separate class to visualize the atoms.

We differentiate between three types of gold atoms, corresponding to the role they play in the simulation. In Figure 2.4 a snapshot of the simulation shows the different atom types. First, there are *normal* gold atoms (drawn in blue), that only feel the forces of the other atoms through Equation 2.3. Then, there are *boundary* atoms (drawn with green and red). These are gold atoms that feel an additional force to confine their positions. A parabolic potential well for each boundary atom, centered at the place we want it to be, keeps the system fixed by fixing the boundaries. The potential wells mimic the presence of atoms beyond the boundaries. This approach allows dynamics even for the boundary atoms, making it possible to apply a thermostat and have realistic interaction with the other normal gold atoms. There are two types of such boundary atoms: tip boundary atoms and surface boundary

[33] Fabrizio Cleri and Vittorio Rosato. In: *Phys. Rev. B* 48 (1993), p. 22.

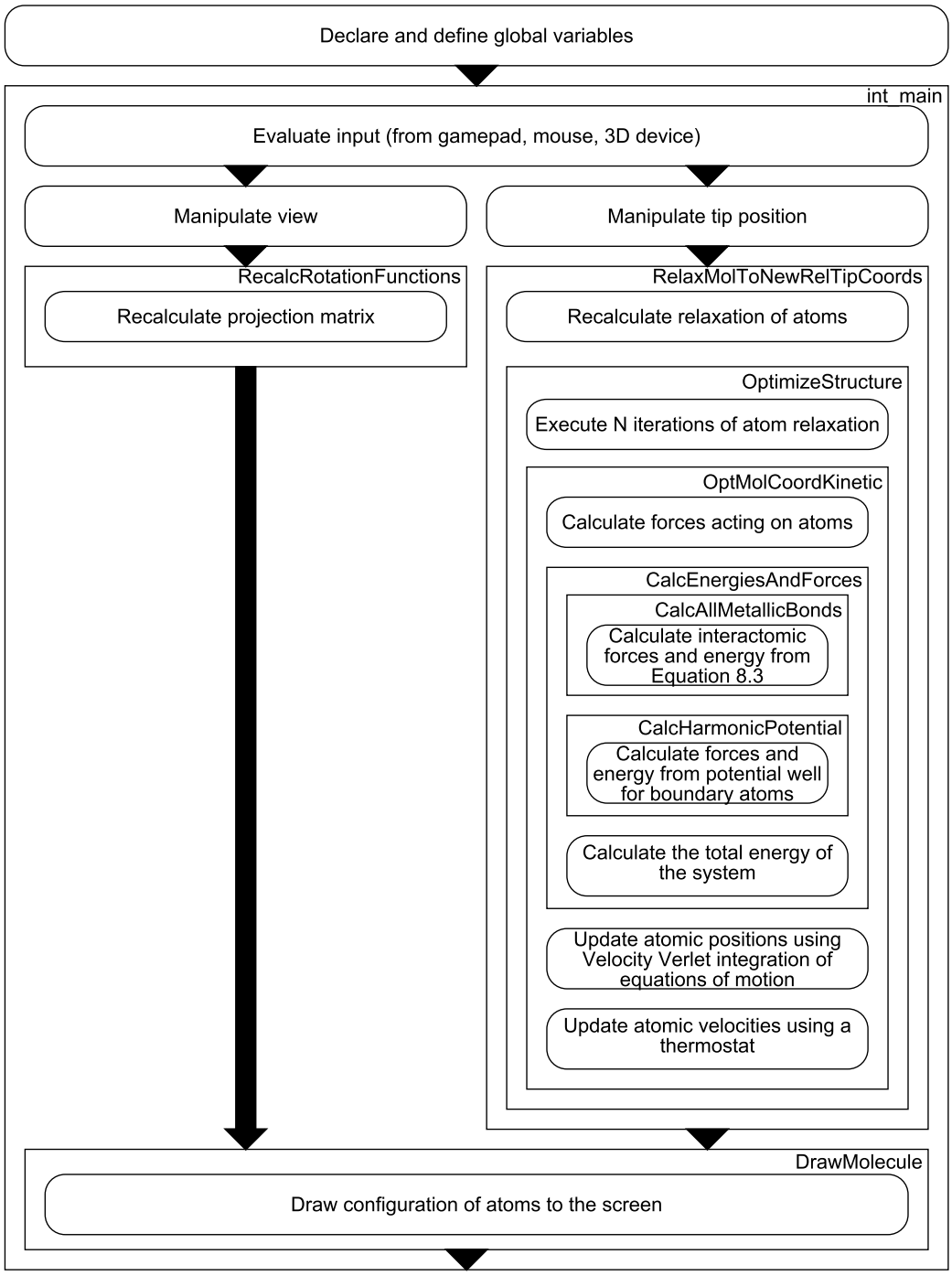

Figure 2.3: Schematic flowchart of simulation execution. Functions are represented by rectangular boxes with their name in the upper right corner. The actions they perform are shown in the boxes with round edges.

atoms. For surface boundary atoms, the position of the potential well stays the same throughout the simulation. For tip boundary atoms, the position of the potential well can be changed to simulate tip motion. As there is a huge discrepancy in time scales between experiment and simulation, a tip motion of some Å in several seconds in experiments happens within picoseconds in the simulation, yielding a much higher tip velocity and acceleration in the simulation. This large amount of kinetic energy pumped into the system has to be drained out using a suitable thermostat. A Berendsen thermostat[34] is implemented into the simulation, which provides a gradual temperature decay instead of sudden re-scaling. Here the instantaneous temperature changes proportional to the temperature difference with the reference temperature T_0 with an adjustable coupling to a heat bath.

$$\dot{T} = \tau_{\mathrm{B}}^{-1}(T_0 - T(t)) \tag{2.4}$$

where τ_B is the temperature relaxation time, related to the strength of the coupling. The velocities of all atoms are rescaled at every timestep (Δt) with the same factor

$$\lambda_{\mathrm{B}}(t) = \sqrt{1 + \frac{\Delta t}{\tau_{\mathrm{B}}}\left(\frac{T_0}{T(t)} - 1\right)} \tag{2.5}$$

A typical value for τ_B in condensed systems is of the order of 0.1 ps[35]. In our case only the boundary atoms are subject to temperature control by a thermostat. This way kinetic energy is transferred through the normal atoms to the boundary atoms, where temperature is controlled, as is also done by Henriksson *et al.*[36]. In order to prevent strongly disturbing the system a special procedure is used to displace the tip boundary atoms. By simply moving the potential wells, the tip boundary atoms would feel strong forces and acquire high velocities. As described above, this amount of kinetic energy would be problematic for the thermostat to dissipate. Instead, we change the position of the tip boundary atoms and their potential wells simultaneously by directly adding smooth displacements. This way, they will change position without additional velocity, and therefore they will not acquire a high temperature. The thermostat then only has to take care of the velocities induced by interactions with the normal atoms in the tip.

2.3.2 Speed-up techniques

Several optimizations and approximations are implemented to speed up the computation so that the simulation can run in real-time. First, we introduce a cut-off radius of 7 Å in the calculation of forces and energy between pairs of atoms. The exponential functions from Equation 2.1 are computationally heavy ; a cut-off radius reduces the number of exponential functions that are calculated. If r_{ij}, the distance between two evaluated atoms, is larger than the cut-off radius, this pair of atoms will not be taken into account in the energy and force calculations. Because of the exponential decay with distance in the potential, their contribution is very small. As described in the

[34] H. J. C. Berendsen et al. In: *The Journal of Chemical Physics* 81 (1984), p. 3684.
[35] Philippe H. Hünenberger. In: *Advanced computer simulation* (2005), p. 130.
[36] K. O. E. Henriksson et al. In: *Phys. Rev. B* 71 (2005), p. 014117.

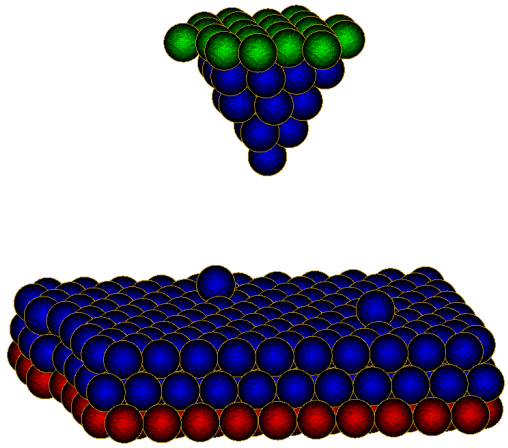

Figure 2.4: Snapshot of the Molecular Dynamics Simulation showing the different atom types. *Normal* gold atoms are drawn in blue, *tip boundary* atoms in green and *surface boundary* atoms in red.

book by Andrew Leach[37], just using a force cutoff would not give a decent speed-up as to use a force cutoff radius one has to compute first all the atomic radii (which involves evaluating a square root which is also computationally expensive) and then measure the forces only within the cutoff radius. In the system we study through molecular dynamics, most of the atoms don't change their nearest neighbours very often and so we introduce another cut-off radius, now for the calculation of the distances between atoms. The other possibility is to use a Verlet's nearest neighbour list, which also requires creation and update of at least two extra arrays (a nearest neighbour array and a pointer array).

Moreover, we do not need to know the distance between atoms that are far apart, since their contributions will not be taken into account because of the cut-off radius for forces and energy. Therefore we only update inter-atomic distances at every simulation step if the previous distance was smaller than a cut-off radius of 7 Å. The larger distances are updated less frequently: only once every 50 simulation steps. Secondly, we implement a lookup table to increase the calculation speed of the exponential functions that still need to be found. This means that the exponential function is evaluated for a long list of relevant inter-atomic distances at the initialization of the simulation. Every time it needs to be calculated during runtime, a linear interpolation of the pre-calculated values around the given distance is used instead of calculating the exponential itself. Looking up the value from the lookup table is faster than calculating it, resulting in better performance. We have compared this speed up in simulation due to the aforementioned approximations with a standard implementation of the MD simulations without any approximations. For this we performed a structural relaxation step in a system analogous to the one shown in Figure 2.4 and checked the difference in the final relaxed state total energy between our method and

[37] Andrew R. Leach. Molecular modelling: principles and applications, Pearson education, 2001.

a conventional approach. We found that the error in final total energy induced by the cut-off radii and lookup table is very small (approximately 10^{-4} percent), while the speed up of almost 10 fold in energy and force calculation is recorded by a standard profiling tool.

A supporting program has also been developed to setup a simulation stage based on the STM images taken during the experiment prior to the start of the main program. To prepare an exact stage as in the experiments, it requires not only the exact knowledge of the positions of ad-atoms on the surface but also the atomic configuration of the surface and the STM tip. Standard STM images of Au(111) surface can provide the information about the crystallographic directions from the Herringbone reconstructions[3] or atomically sharp step edges and the location of FCC or HCP packing. The atomic configuration of the metallic surfaces like Au(111) is not readily available in STM images (see Figure 2.2(b)) due to the delocalized nature of the valence electrons in metals[38]. It is possible to image the atomic configuration by functionalizing the STM tip by adsorbates (for example CO molecules)[39]. To keep the surface clean we did not introduce impurities in the system and we devised a simple geometric technique (explained in the next section) to get the information of the surface atoms positions without the need to resolve the individual surface atoms. The atomic shape of the tip is always an unknown quantity in STM. Although one could obtain partial information before the start of the experiment using field ion microscope (FIM), but after a few manipulations steps the tip shape would become unknown. We developed a localized tip shaping procedure published elsewhere[29] which helps in preparing a crystalline tip apex up to the second atomic layer from the apex atom. A brief description of this work is given in Appendix D.

2.4 Experimental measurements

In this section we will show how the above system with the real-time MD simulation works using some simple lateral manipulation test followed by an experiment where we lifted a chain of Au atoms out of the surface in a controlled manner forming a free standing atomic chain between the tip and the sample. Some challenges in creating such a free standing atomic chain using a controlled STM technique are addressed by Tartaglini *et al.*[40]. These atomic chains are ideal 1D systems and are known to be formed only in pure metals like Au, Pt and Ir metals. They derive their origin from relativistic effects[41][4] which cause a contraction of the s-shell and increases its occupation at the expense of the d-electrons. This leads to strengthening of the d-bond and thus a higher stability to form atomic chains. These chains have been studied experimentally using statistical methods like MCBJ[20,42] and STMBJ[43]

[3] Herringbone surface reconstructions have a 120 degree spatial symmetry and run perpendicular to the crystallographic directions

[4] For detail explanation, see reference Agraït *et al.*[41] and the references therein

[38] J. Wintterlin et al. In: *Phys. Rev. Lett.* 62 (1989), p. 59.
[39] N. J. Zheng and I. S. T. Tsong. In: *Phys. Rev. B* 41 (1990), p. 2671.
[40] E. Tartaglini et al. In: *Low Temperature Physics* 39 (2013), p. 189.
[41] Nicolás Agraït et al. In: *Physics Reports* 377 (2003), p. 81.
[42] A. I. Yanson et al. In: *Nature* 395 (1998), p. 783.
[43] Hideaki Ohnishi et al. In: *Nature* 395 (1998), p. 780.

where two macroscopic size electrodes are pulled apart until the last atom contact is formed and then on further pulling of the junction new atoms from the leads join thereby forming atomic chains. From an atomistic point of view, the reason why new atoms from the bulk (where they are having more than one bond with other atoms) are pulled out to form an atomic chain can be understood by the fact that in metals the bond strength increases as the coordination number is decreased. This causes a single linear bond to become comparable to three bonds (for gold) in the bulk. Since our MD simulation uses an embedded atom potential which measures pair interactions, the effect of coordination number is automatically accounted for within the approximate atomic interaction force.

Another interesting phenomenon from the electronic point of view that was also found experimentally[20] was that the conductance of these atomic chains oscillates as function of number of atoms in the chain and this effect is known as 'parity oscillations'. These oscillations were explained (Reference Agraït *et al*.[41] and Cuevas *et al*.[44] and the references therein) as an interference effect occurring due to back-scattering of electronic waves at the interface between the bulk and the atomic chain. This back-scattering makes this phenomena similar to the Fabry-Pérot interferometer in optics. This was demonstrated in experiments by making length histograms[20] of conductance and it was observed as oscillations in conductance. Therefore free standing atomic chains can be used to test our set up, and the formation of chains can be checked by the observation of parity oscillations.

2.4.1 Obtaining the positions of the background substrate atoms

At the start of the experiment we deposit single Au ad-atoms on the middle of the FCC sector of the herringbone reconstruction on a clean Au(111) surface with the STM tip as explained earlier (Section 2.2). Then a simulation has to be prepared with the ad-atoms lying on the exact same atomic configuration on the surface as in the experiment. To get the information about the background atoms (without functionalizing the tip), we use a geometry based technique. After our surface preparation we can get directly from the orientations of the straight step edges (Figure 2.2(a))[5] the angle of the three crystallographic directions (shown with white lines) in our STM images. Once the three crystallographic directions are established [6] the next step is to find out whether the ad-atom sits on the left (L) or right (R) of the triangular hollow site (shown in Figure 2.5(a)) .

This means that within a linear translation of the lattice, there is a 50% chance of being correct if we choose one of the two hollow sites (L or R). But in fact with the help of just two ad-atoms and a geometric argument we could tell with 100% certainty the position of both the ad-atoms and have a complete information about the background atoms. If we take any two ad-atoms placed near to each other in the experiment, they could be lying either on similar orientated hollow sites (LL or RR) or opposite oriented

[5] These steps appear after locally distorting the surface by tip indentation at a place remote from the measurement location

[6] The crystallographic directions of the surface locally can also be obtained using the angles of the Herringbone reconstruction in (111) surfaces provided that the location is far from any defect sites or corners of the Herringbone as these can change or alter the orientation locally.

[44] Juan Carlos Cuevas and Elke Scheer. Molecular electronics : an introduction to theory and experiment. New Jersey [u.a.] : World Scientific, 2010.

hollow sites (LR or RL). We overlay the measured STM image with the known lattice periodicity, as shown in Figure 2.5. If they are placed on the opposite oriented hollow sites (as shown in Figure 2.5(b)), then within the translational symmetry of the background lattice there is only one possible orientation: either we find that the top left atom sits in the L site and the lower right one in the R site, or the other way around. For example if we try to translate the background lattice scheme such that the bottom right ad-atom in Figure 2.5(b) shifts from the R hollow site (where it is lying) to a L hollow site as shown in Figure 2.5(a), then one can see that the top left ad-atom does not fit anymore in any hollow site. This shows that only the positioning of the ad-atoms shown in Figure 2.5(b) is correct. On the other hand if they are placed on similar hollow sites (LL or RR), then it is not possible to directly conclude their positions by doing the linear translation described above. The solution is to perform one atomic manipulation move of one of the two ad-atoms to bring them in the opposite oriented hollow sites.

This elegant and accurate approach allows us to determine the background lattice without the need to work towards atomic resolution of the Au(111) surface each time. The method is not only limited to the Au(111) surface but a similar geometrical argument can be used on other surfaces as well, and it can be used to determine the binding sites of deposited molecules. An approach by tracking an ad-atom movement to get the information about the background lattice has been reported earlier by Böhringer *et al*.[45]. Currently available techniques for determining surface atomic configuration using STM are either based on functionalising the STM tip with another molecule (like CO) or by doing point contact scanning[46]. After having determined the structure of the background lattice and the position of the ad-atoms with respect to it, the next step is to construct a simulation stage which has the same structure as in the experiment.

2.4.2 Point contact pushing

We start now our experiment in the configuration shown in Figure 2.6(a) and the corresponding simulation picture in Figure 2.6(d). Usual lateral manipulation[5–7](LM) is done by keeping a tunnel gap between the tip and surface (or ad-atom) operating in a constant current mode with feedback loop switched on. Different settings of the tunnel resistance can lead to different modes of manipulation. For example for gold the numbers reported[28] are 150 kΩ for pulling, 330 kΩ for pushing and 500 kΩ for quasi (near) sliding. In our case, manipulation can be started in a new point contact pushing (PCP) mode with feedback loop switched off. The difference between our PCP mode and usual LM modes is that we do not move the tip in a straight path but we move from hollow site to hollow site by bringing the tip always in-line with the path to the next hollow site and then push the ad-atom. This is done so that the ad-atom position can be known and controlled at each step of the manipulation and avoids the complex jumps and movement of the ad-atom depending on the relative alignment of the underlying lattice and the manipulation direction[47].

In our manipulation method we first perform a tip height match between the simulation and the experiment by going above an ad-atom in point contact in the

[45] M. Böhringer et al. In: *Surface Science* 419 (1998), p. L95.
[46] Yong-hui Zhang et al. In: *Nano letters* 11 (2011), p. 3838.
[47] Saw-Wai Hla et al. In: *Phys. Rev. B* 67 (2003), p. 201402.

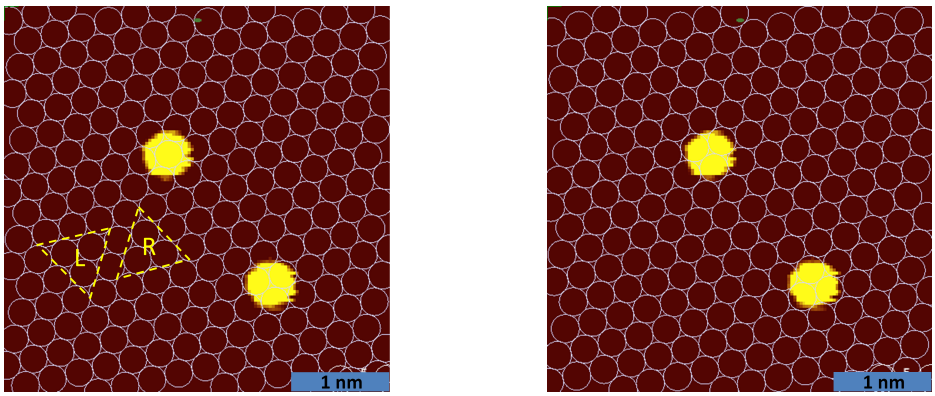

(a) (b)

Figure 2.5: Determination of substrate atoms configuration via geometric argumentation. The two panels show the STM images with the topography color scale tuned to reduce the apparent size of the two ad-atoms to match the superimposed background lattice pattern. The actual apparent size of Au ad-atoms on Au(111) is around 1 nm as shown in Figure 2.2(b). The right image with one atom on 'L' and the other on 'R' is showing the correct positioning of the ad-atoms with reference to background lattice.

experiment resulting in a jump to contact and a stable level at 1 G_0 conductance. This is different from some previous works which have shown that a jump to contact occurs only when approaching a bare metallic surface, while when approaching an ad-atom on the surface there is a smooth transition from tunnelling to contact[48,49]. This absence of a jump to contact has been attributed to an increased bond strength of the adsorbed atom on the surface because of the surface dipole creation due to the Smoluchowski effect. We have very rarely seen a smooth transition to contact and we attribute those rare events to either a blunt tip or to the presence of unwanted adsorbates which were present in the UHV chamber, most likely hydrogen. In fact we have observed this jump to contact when approaching a Au ad-atom from the top more than 80% of the times and we attribute it to the relaxation[50] of tip and surface atoms. At this point, after matching the contact position of the tip in both simulation and experiment we retract the STM out of contact and position the tip about 1 nm "behind" the ad-atom, at a height corresponding to 0.4 μA tunneling current at 100 mV bias (which is around 250 kΩ tunnel resistance and approximately 1.2 Å above the surface). Then the tip is moved towards the ad-atom in feedback-off condition keeping z constant. Similar to the jump to contact (JC) phenomenon that happens while approaching a surface or an ad-atom from the top, a JC also occurs while approaching the ad-atom laterally parallel to surface. Because the corrugation energy in metallic surfaces is usually 1/10 to 1/3 of the adsorption energy[2], this jump

[48] J. Kröger et al. In: *New Journal of Physics* 9 (2007), p. 153.
[49] L. Limot et al. In: *Phys. Rev. Lett.* 94 (2005), p. 126102.
[50] W. A. Hofer et al. In: *Phys. Rev. Lett.* 87 (2001), p. 236104.

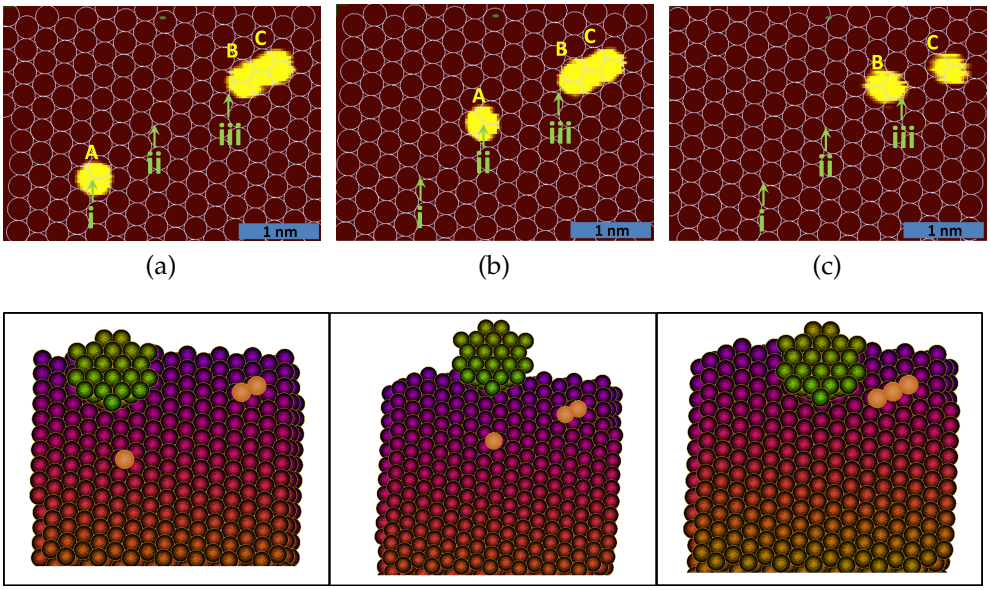

Figure 2.6: The top three panels show the STM images with the topography color scale tuned to show a smaller apparent size of the ad-atoms 'A', 'B' or 'C'. The scale bar in the bottom-right corner is 500 pm. The bottom three panels show the corresponding simulation setup. (a),(d) shows the initial positions of ad-atoms 'A', 'B' and 'C' with 'A' at position 'i'. (b),(e) shows the position of ad-atom 'A' after the first move and one can see that the ad-atom arrives at the exact same position 'ii' in both experiment and simulation. (c),(f) shows the STM image and simulation after the gold atomic chain has been lifted.

can even be larger in the lateral direction than while approaching from the top. We used this procedure to first move the ad-atom 'A' shown in Figure 2.6 from position 'i' to 'ii' and then a STM image (Figure 2.6(b)) is taken so that one can compare the position of the ad-atom with the simulation (Figure 2.6(e)). The motion control and visual feedback from the simulation are essential in this procedure, because we need to move the tip in a zig-zag fashion behind the atom in the line of the next hollow-to-hollow hop for each lattice step. The resulting positions in Figure 2.6(b) and (e) match very well.[7].

2.4.3 Lifting of gold atomic chain

In the second step, we start now from position 'ii' and move the ad-atom 'A' to position 'iii' and then continue with the operation of lifting-off the atomic chain followed by taking the STM image at the end(Figure 2.6(c)). Figure 2.7(a) shows the tip trajectory[8] for the second step and Figure 2.7(b) shows the corresponding conductance and Z

[7] The corresponding x, y, z and x, y, G curves for this operation are given in the Appendix A.2
[8] The corresponding x, y, G graph for this operation is given in the Appendix A.2

coordinate variation over the time. The points from 1-10 shown in the two graphs mark the same points in time. A schematic explaining the manipulation process is given in Figure 2.7(c). Starting points 1 to 4 show the start operation which includes the tip height matching and positioning the tip behind the ad-atom as explained in section 2.4.2. After this the tip is moved forward (keeping the Z constant) in feedback-off state towards the ad-atom. Next, a lateral jump to contact happens[9], which gives a sudden change in conductance to approximately 1 G_0, as can be seen from point 5 to 5′ in Figure 2.7(b).

Next the ad-atom is moved towards the other pair of atoms 'B' and 'C' to position 'iii' going from one hollow site to the next hollow site (L to R or R to L) shown as the meandering part in Figure 2.7(a) from point 5′ to 6. Now after the ad-atom 'A' has reached position 'iii' the tip is controllably moved from point 6 to point 7 shown Figure 2.7(a) and (b). This places the ad-atom 'A' above ad-atom 'B' which together with the tip-apex atom[10] forms a three atom chain as shown in Figure 2.7(c). This causes a decrease in conductance which can be seen clearly in Figure 2.7(b). Note that the Z-position in Figure 2.7(b) shows at point 7 the 'Z' value of 0.45 nm, and adding to this 0.12 nm (which is the Z=0 point given by the tip height from surface during pushing) gives 0.57 nm, which is very close to twice the covalent diameter[11] of a single Au atom (i.e. 0.288 nm). After keeping the tip at this position for some time we bring the ad-atom 'A' back to the surface (point 8). The number of atoms in the chain changes back from three to two giving a step increase in conductance, shown in Figure 2.7(b). Note that this conductance value (point 8) is lower than the earlier value between points 5′ and 6. The difference results from the fact that between point 5′ to 6 the tip is not above the ad-atom 'A', but is actually on its back in a pushing mode. Thus the overlap of the wave functions on the atomic chain and those in the tip are enhanced at this position, giving rise to a higher transmission and conductance. Then we bring the ad-atom again 'A' above the ad-atom 'B' (making a three atom chain) and we see again a conductance drop to exact same value as earlier (point 9 in Figure 2.7(b)).

Eventually, when attempting to pull the tip further expecting the ad-atom 'C' to join-in the chain, the chain broke. The STM image taken at the end (Figure 2.6(c)) shows two ad-atoms left on the surface, supposedly 'B' and 'C'. The positions of 'B' and 'C' have changed but the exact sequence of steps that led to those movements cannot be determined because our simulation didn't follow the experiment after point 6. In the experiment, the ad-atom 'A' was moved above the ad-atom 'B', while in the simulation the trimer('A-B-C') was left on the surface once the tip was pulled up (Figure 2.6(f)). A possible reason why the simulation did not follow the experiment is that the atomic shape of the actual tip apex was possibly different from the crystalline one which we assumed in our simulation. This would lead to a different shape of the double potential well making the potential well for the tip used in the experiment deeper than the one on the surface side. Thus, breaking the ad-atom bond to the

[9] Note that a lateral jump to contact will also occur when ad-atom 'A' is brought closer to ad-atom 'B', but as 'B' and 'C' are very close the jump of 'B' towards 'A' should be very short range.

[10] We have developed a robust procedure to prepare STM tip apex structure using mechanical annealing procedure described in Appendix D. This helps us in confirming an atomically sharp tip structure up to the second atomic layer behind the tip-apex atom.

[11] https://www.webelements.com/gold/atom_sizes.html

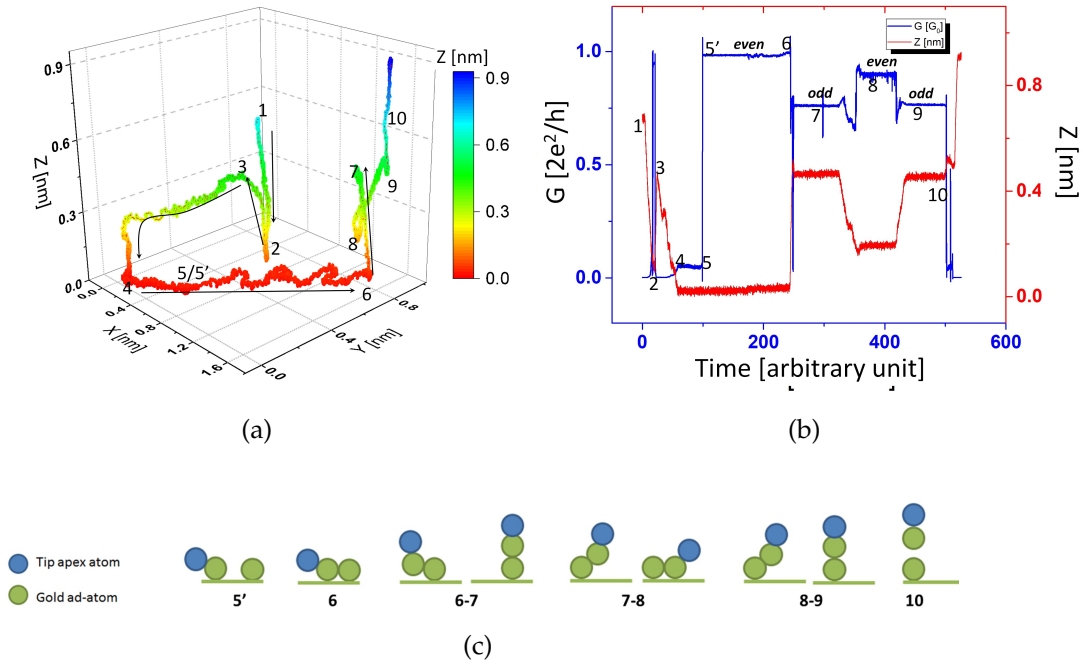

Figure 2.7: (a) Complete tip trajectory for the second step starting from position 'ii' in the lattice and (b) variation in conductance (blue) and Z coordinate (red) of the tip over the time of operation. The numbered points shown in the two graphs (a) and (b) correspond to the same points in time. (c) Schematic of the manipulation process explaining different points in the curves above.

surface becomes easier as compared to that in the simulation. Another explanation could be that our simulation does not take into account excitation of the substrate ad-atom vibration modes due to inelastic electron tunneling[17,51], which is expected to promote pick up of the ad-atoms from the surface. Finally, of course, the effective atom-atom interaction employed for the simulation is a crude approximation for the true interatomic potentials, and this approximation may break down for these extremely under-coordinated atoms.

2.4.4 Parity oscillations

The conductance of a macroscopic conductor decreases with increase in its length. However in small atomic scale devices due to the ballistic nature of electronic transport, the conductance should not change with the length of the device. However, chain length dependent oscillations in the conductance in mono-atomic chains have been reported by the name of parity oscillations or even-odd oscillations. Experimentally in gold atomic chains, such parity oscillations are demonstrated by making length histograms using a mechanically controlled break junction (MCBJ)

[51] Phaedon Avouris. In: *Accounts of chemical research* 28 (1995), p. 95.

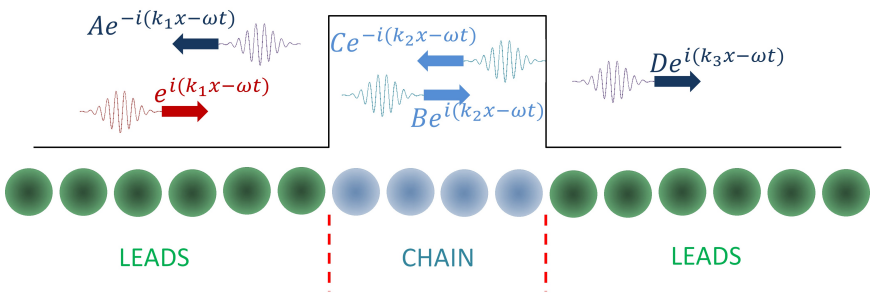

Figure 2.8: A one-dimensional model of electronic transport through a mono-atomic chain[53]. To differentiate between the atomic chain and the leads, a different wave-vector k_2 is allotted to the chain as compared to k_1 and k_3 for the leads. This difference in wave-vector can be manifested as a potential barrier and the electrons form standing waves inside the barrier. Depending on the length of the barrier one can have different interference patterns of these standing waves giving oscillations in the conductance. This is similar to a Fabry-Pérot interferometer. The different colours of atoms here do not imply different types of atoms but are used only to differentiate between the leads and the atomic-chain.

setup[20,52,53]. These oscillations can be explained using a simple one-dimensional (1D) chain model (description given in the Figure 2.8) and its existence has been confirmed also by various detailed theoretical calculations[20,54–58]. However, there is a disagreement about the phase of these oscillations among different models. The phase defines whether the conductance of the chain with an even number of atoms will be larger than that of the chain with an odd number of atoms, or the other way around. A phase change can arise with the type of monovalent atom forming the chain (alkali metals or noble metals)[58] but can also arise due to the geometrical shape of the electrodes[57] and the coupling between the electrode and the atomic chain[56].

The controlled experiment described in Figure 2.7 not only shows clearly these even-odd oscillations but also fixes their phase. We can determine here with certainty that the even number of atoms in the chain leads to a higher conductance. As compared to previous experimental results on gold atomic chains obtained using the MCBJ technique, we have well-defined electrode shapes. One of the electrodes is an atomically flat Au(111) FCC facet and the other electrode is an atomically sharp tip apex prepared using the mechanical annealing technique[29].

[52] R. H. M. Smit et al. In: *Nature* 419 (2002), p. 906.
[53] R. H. M. Smit. PhD thesis. Leiden Institute of Physics (LION), Leiden University, 2003.
[54] N. D. Lang. In: *Phys. Rev. Lett.* 79 (1997), p. 1357.
[55] Mads Brandbyge et al. In: *Phys. Rev. B* 60 (1999), p. 17064.
[56] Rafael Gutierrez et al. In: *Acta Physica Polonica. Series B* 32 (2001), p. 443.
[57] P. Havu et al. In: *Phys. Rev. B* 66 (2002), p. 075401.
[58] Y. J. Lee et al. In: *Phys. Rev. B* 69 (2004), p. 125409.

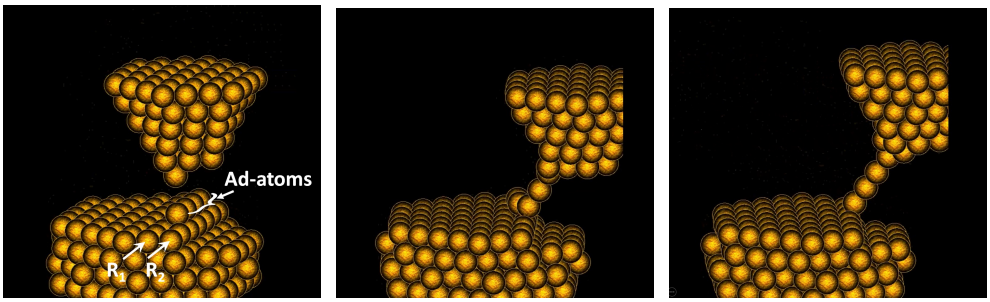

(a) (b) (c)

Figure 2.9: (a)-(c) The sequence of the lifting a gold atomic chain at a step edge. The row of atoms forming the last row of a step edge is labeled as 'R_2' and the row behind it is labeled as 'R_1'. Four ad-atoms are placed at the step edge, which are lifted off the surface by the tip, forming suspended chain.

2.4.5 Lifting of a gold atomic chain along a step edge

As the discrepancy between the experiment and the simulation due to lack of knowledge of atomic configuration of the tip cannot be easily overcome, the following question rises: Is there a possible configuration of tip-ad-atom-surface system or a possible trajectory of the STM tip where even with the tightly packed crystalline tip assumed in the simulation, one could lift a chain of atoms? With the help of the MD simulations we found that if the chain of atoms can be prepared along the step edge in a crystalline direction, then even with the crystalline tip and a suitable tip trajectory this chain could be lifted off the surface, as shown in Figure 2.9 (a)-(c). This result may seem counter-intuitive as it is known that the step-edges are more reactive (that is the reason why adsorbate molecules are pinned to them) because of the under-coordinated row of atoms on the step edge. Figure 2.9 (a) shows a row of four ad-atoms lying parallel to the step edge. The last row R_2 below the 4 ad-atoms has no atoms on its right, which means that they are less co-ordinated and thus make a stronger bond to the 4 ad-atoms. However, the procedure to lift the chain of four atoms off the surface is not to go vertically up trying to break three bonds at the same time but rather first pull the ad-atom to the right, in the direction of the lower plateau (as shown in Figure 2.9(b)). Next, once the bonds with the row R_1 are broken then on going vertical the ad-atom can be pulled out. On applying a similar procedure for detaching the next atoms in the chain a free standing atomic chain between the tip and surface can be obtained (Figure 2.9(c)) even with for the limitations imposed by the simulation.

We set out to prepare such an atomic chain on a step edge in the experiments, but this turned out not entirely trivial. The major hurdles for doing so are: First, as the Herringbone reconstruction on Au(111) is known to end perpendicular to the crystalline step edges, the chain has to be prepared along the width of the FCC region rather than along its length as before. Secondly, as explained above, a lateral jump to contact will occur while bringing the second ad-atom to the step edge and this will lead to dimer creation mostly in the crystallographic direction of the incoming ad-atom, which will be most likely different from the crystallographic direction of

step edge. A possible way around could be to make something similar to what was prepared by Nazin et al.[59] on the NiAl(110) surface i.e., a "metallic chain - molecule - metallic chain" system. Bringing a molecule on the step edge first and then attaching Au atoms on its end to form a chain is a possible way to avoid this lateral jump to contact.

2.5 Discussion

In the previous section we showed that we were able to controllably form a free standing atomic chain, put it back down on the surface and lift it up again. Furthermore we have observed clear parity oscillations as a signature of the atomic chain formation. In this paragraph we will address the effect of the shape of the tip in these experiments. Any modification of the tip apex atom position with respect to the bulk of the tip during manipulation should influence the accuracy and the outcome of the manipulation. In spite of this, formation of complex 2D structures[3,9–15] are reported in the past with lateral manipulation technique with precise positioning. However, the accuracy and error in this positioning step are generally not reported. It is possible that recursive methods were used as reported by some groups[14,15], where multiple iterations were done to finally converge to a pre-determined position.

Another important item that will play a role in lateral manipulation (other than tip apex atomic structure) is the assumption of isotropic spring stiffness of the tip. To study the effect of the spring stiffness on manipulation, one can project it (as shown in Figure 2.10) along the crystallographic directions of the surface (three in case of Au(111) surface). In case of a real tip structure it is possible that the three projections (κ_1, κ_2 and κ_3) of the stiffness along the three crystallographic directions of the surface (1, 2 and 3) are not the same. This implies that the lateral deflection of the tip apex atom (δ_1, δ_2 and δ_3) during lateral manipulation along different crystalline orientations will be different.

Important to note here is that for harder materials like Tungsten (W) which is used as a tip material in many atomic manipulation experiments, the three tip stiffness constants(κ_i's) may be very large and so even though the deflections (δ_i's) are possibly different, they will be very small to detect. Even for softer materials (like Au or Au covered PtIr tips), due to the quadratic nature of the spring energy ($\frac{1}{2}\kappa_i\delta_i^2$) the spring will deflect only at the start and for longer manipulation distance it will remain almost constant. Therefore, the relative error in the positioning of an ad-atom over the surface (defined as expected position minus the measured position divided by the expected position) can be large for small movements while will become smaller for larger distance. We have investigated the role of this anisotropic spring stiffness. In order to do this we needed to avoid the lateral jump to contact behavior mentioned earlier. For this purpose our 3D motion control system is once more convenient: this time instead of approaching the ad-atom from the side on the surface where we detect the lateral jump to contact, we devised a new routine where we approach the ad-atom from the top, and establish a point contact. Subsequently, we make a quarter circular motion (while keeping in contact with the ad-atom) and thus the tip comes into the pushing position as before without having any lateral jump to contact. A figure to explain this pictorially is given in the Appendix A.3. After this preparation

[59] G. V. Nazin et al. In: *Science* 302 (2003), p. 77.

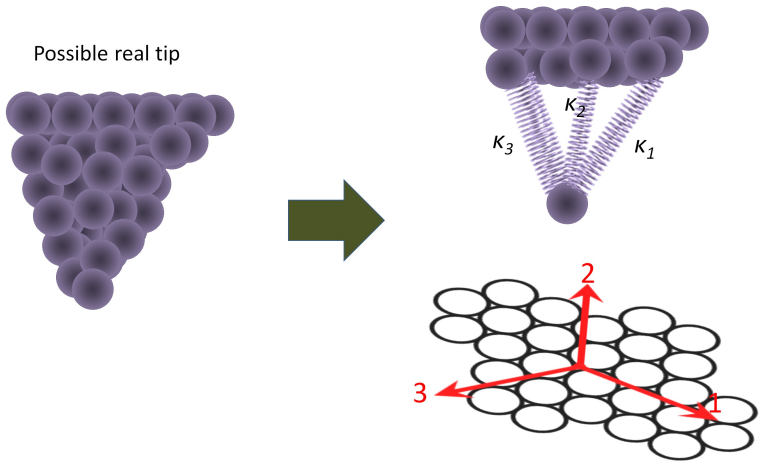

Figure 2.10: A spring stiffness model, showing how an anisotropic tip could have an anisotropic spring stiffness.

procedure we studied experimentally (using randomly formed tip structures) only the single hollow site push occurrences because, as explained before, the major part of the error should happen at the start of the manipulation only. We observed almost 50 % zero error motion. We compared this with single-site displacements made with the molecular dynamics simulation after preparing randomly formed tip structures (produced by a mechanical annealing procedure in the simulation) and found a similar behavior in terms of accuracy. This suggests that the anisotropic lateral spring stiffness[12] of the tip other than the atomic configuration of the tip apex is also an important unknown ingredient which could influence the precision of an atomic manipulation operation.

2.6 Conclusion and outlook

To summarize, we have modified our low temperature ultra-high vacuum STM with the integration of a 3D motion control system and a real-time molecular dynamic simulation. This human-machine augmented system where the operator can become part of the experiment and make adaptable STM tip trajectories based on the visual feedback from simulation, provides a better control for (3D) atomic manipulation. This method should become particularly useful for molecular manipulation. We prepared our surface using local strain induced technique where fresh step edges along crystallographic directions can be formed at cryogenic temperatures. We then showed how a simple geometric technique based on placing two ad-atoms can give information about the atomic configuration of the metallic substrate. We used this as the input to setup the same environment in the coupled real-time simulation and demonstrated the controlled lift-off of single atomic chain. For this purpose, we

[12] In fact the vertical spring stiffness also plays a role. Specially in case of jump to contact phenomena, different vertical spring stiffness should give different conductance values at which the jump occurs.

developed a new point contact pushing technique which can directly be followed by the manipulation into the third dimension at the end. By putting this atomic-chain back and forth into and out of the surface we studied the parity oscillation behavior in conductance which occurs due to interference of electronic waves in different length of the chain. Finally, we also discussed how the spring stiffness of the tip can influence the accuracy of atomic manipulation operations, which is extremely important in complex 3D manipulation of single molecules and atomic chains. The next step will be to modify the real-time simulation to include molecules in the system (see Chapter 3). Experiments on other surfaces like Au(211) can be tried which is not effected by surface reconstructions and still has (111) facets and clean long step edges. For a better comparison with theory and a possible direct feedback loop from the experimental conductance values, a real time conductance estimation based on the atomistic positions given by the MD simulations could be useful. Tight binding models have been known[60] to give a relatively fast (as compared to DFT and other computationally expensive methods) estimation for the conductance values numerically. At the moment we have not added any such electronic transport model in our system but it can be a possible upgrade which should help in further guiding the experiments[61][13].

[13] With the rapid developments in the field of deep learning algorithms[61], an interesting possibility would be to "train" such an algorithm by using many simultaneous force and conductance calculations for varying tip shapes, so that it can find out the exact atomic tip structure used in experiments by studying and recognizing features in conductance traces.

[60] T. N. Todorov and A. P. Sutton. In: *Phys. Rev. B* 54 (1996), R14234.
[61] Jürgen Schmidhuber. In: *Neural networks* 61 (2015), p. 85.